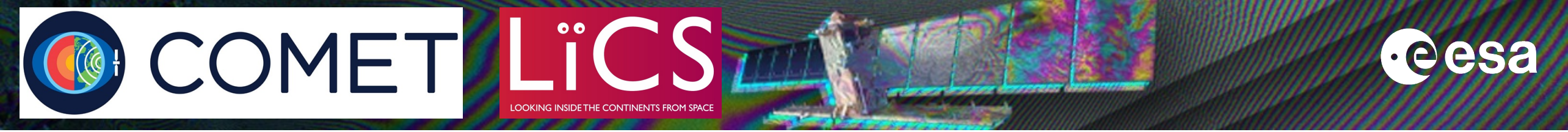

Strain accumulation along the central-eastern Altyn Tagh fault (NW Tibet) from Sentinel-1 InSAR and GPS Data

Dehua Wang, John Elliott, Gang Zheng, Tim Wright, Andrew Watson, Jack McGrath

COMET, School of Earth and Environment, University of Leeds

Email: eedwa@leeds.ac.uk

Motivations

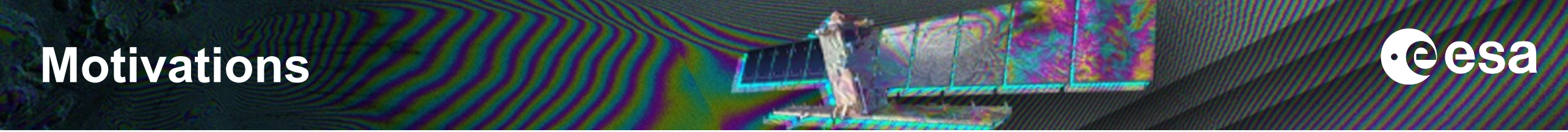

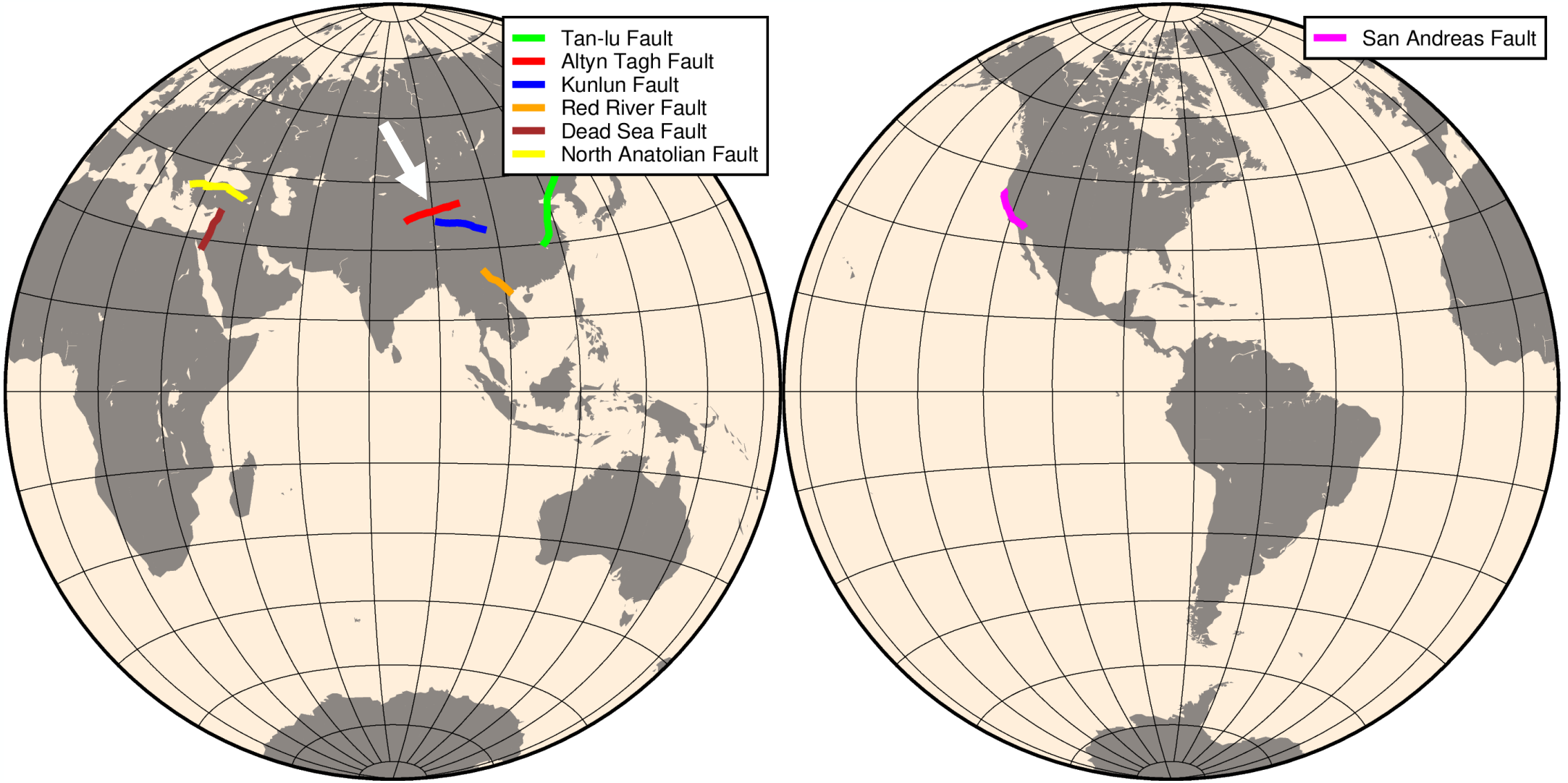

Motivations

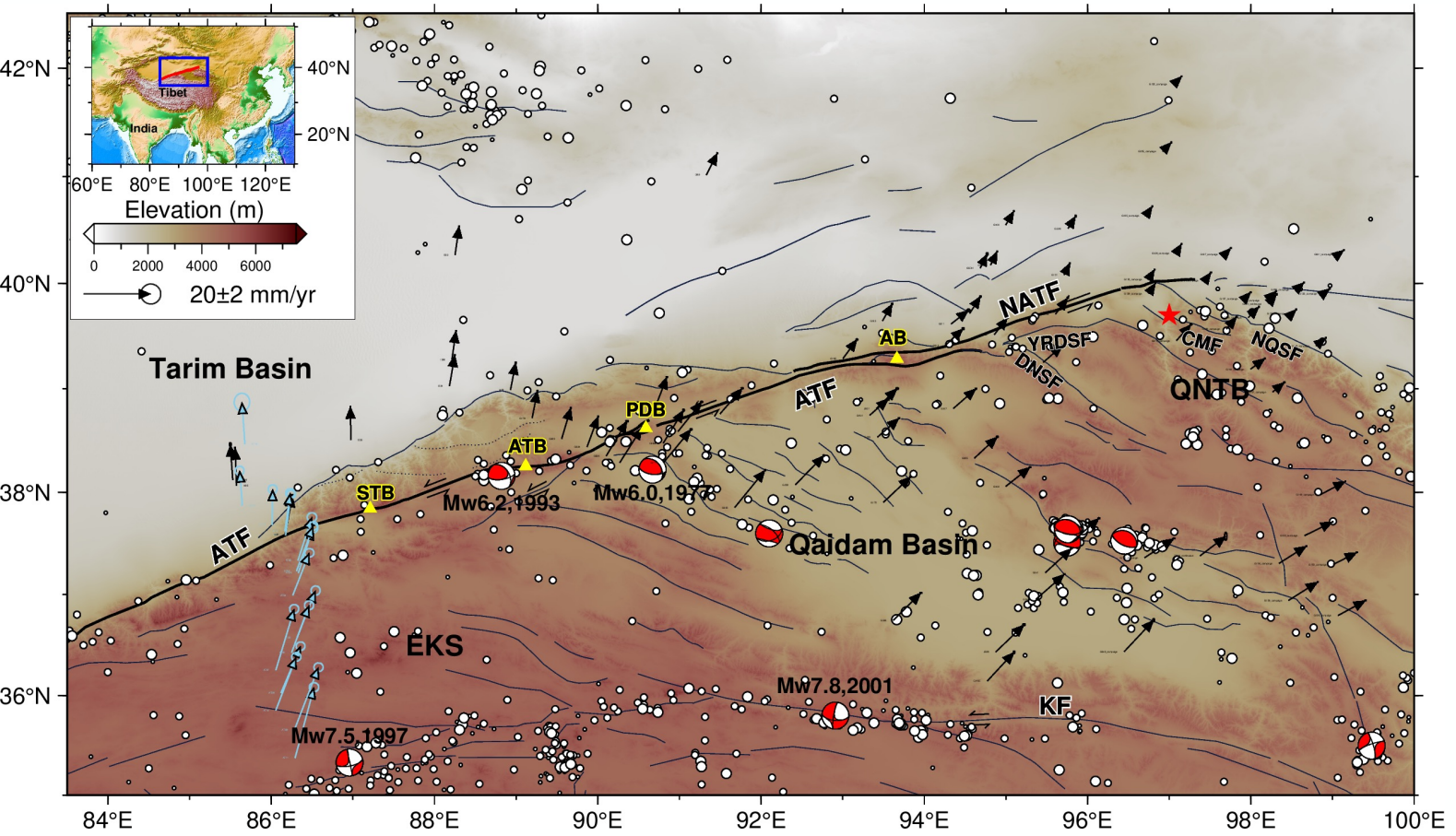

What we pursue?

- **A whole-fault understanding**
- **A 3D velocity map with high spatial resolution**
- **Strain rate maps showing strain rate distribution and potential partitioning**
- **Specific applications:**

★ shear zone location
★ deformation around active fault bends
★ seismic risk evaluation
★ regional mountain building
.....

Data and Methods

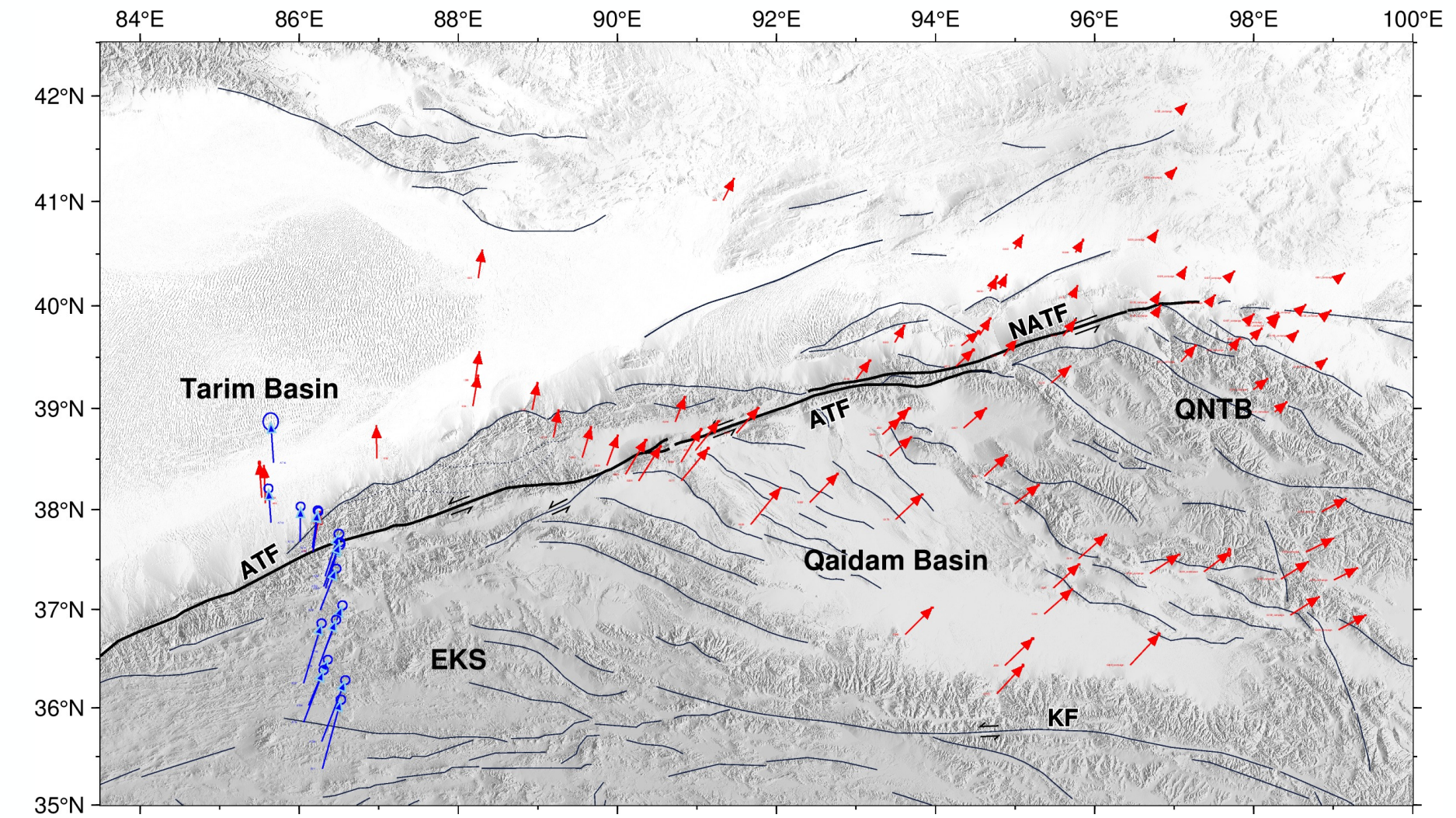

GPS data:

- **78 3D GPS velocities (1998-2021)**
  (New, based on CMONOC-I/II)
- **17 2D GPS velocities (2009-2017)**
  (from Li et al., 2018)

Data and Methods

A frame-based automated InSAR processing system.

Interferograms and coherence maps have been produced using the LiCSAR processor.

Products are multilooked by factors of 5 in the range and 20 in the azimuth directions to achieve a resolution of around 100×100 m per pixel.

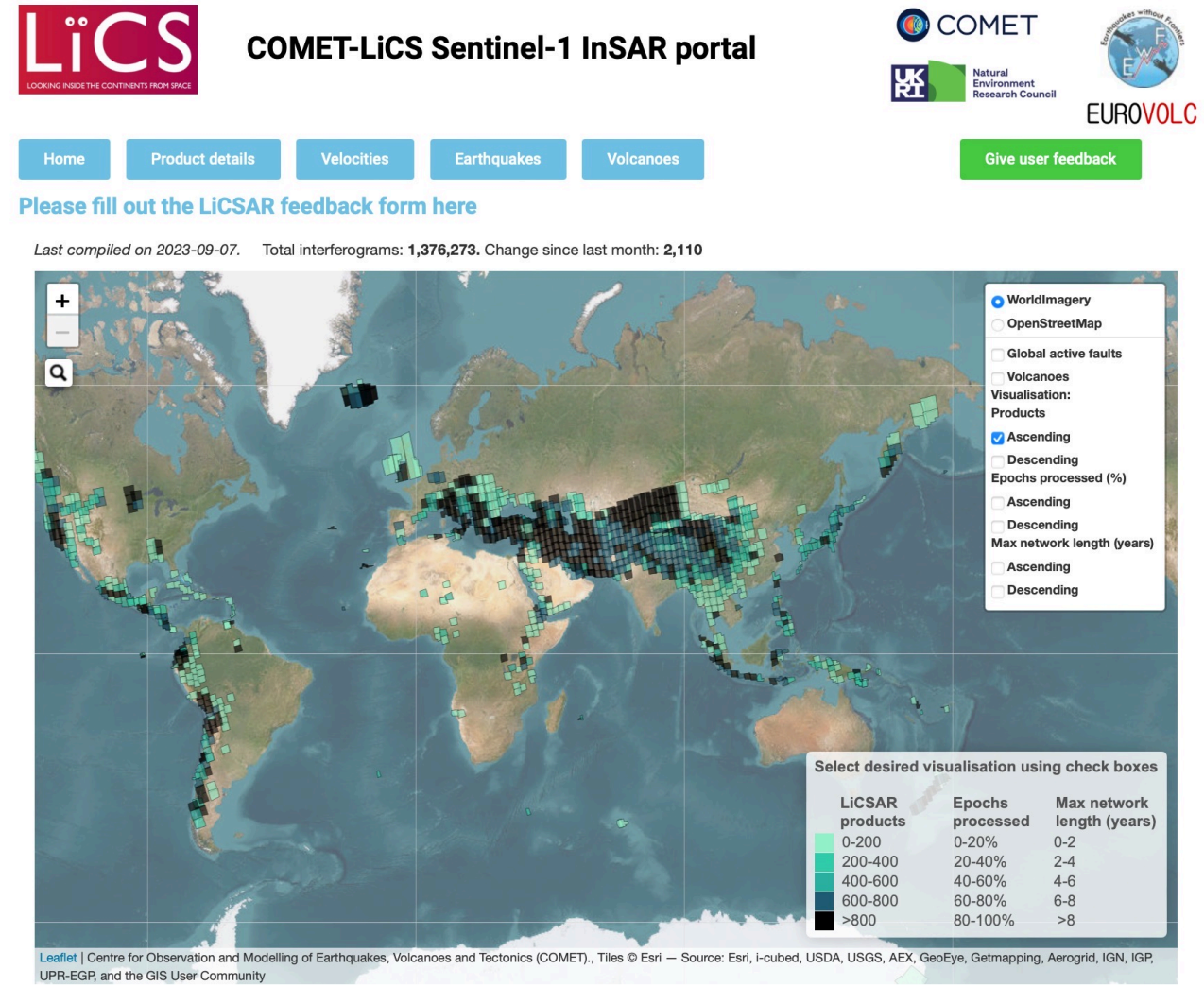

https://comet.nerc.ac.uk/COMET-LiCS-portal/

Morishita et al., (2020). LiCSBAS: An Open-Source InSAR Time Series Analysis Package Integrated with the LiCSAR Automated Sentinel-1 InSAR Processor. *Remote Sensing*, *12*(3), 424.

Data and Methods

Generic Atmospheric Correction Online Service for InSAR (GACOS)

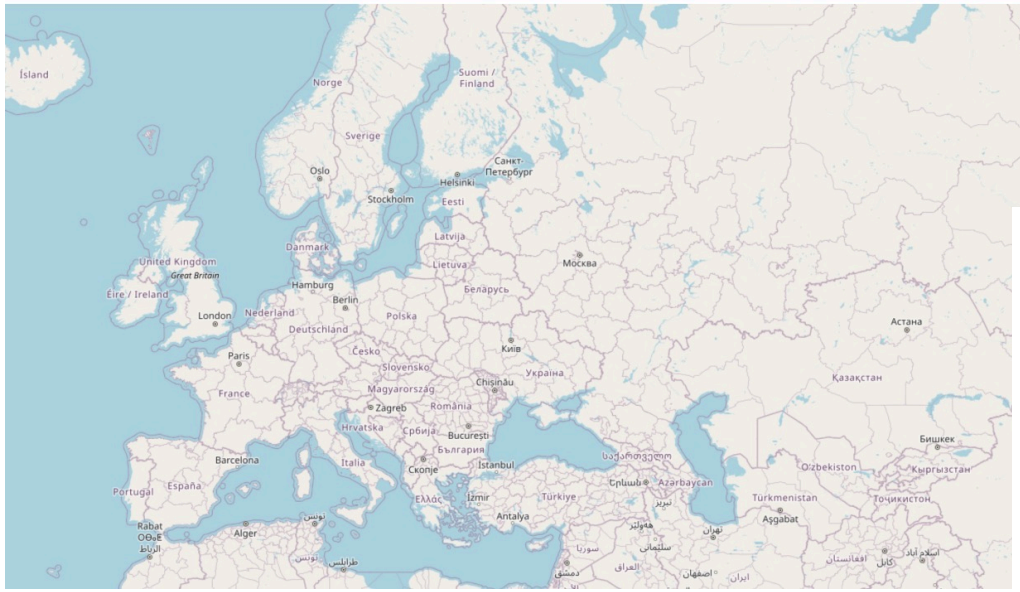

www.gacos.net

Yu, C., Li, Z., Penna, N. T., & Crippa, P. (2018). Generic atmospheric correction model for Interferometric Synthetic Aperture Radar observations. Journal of Geophysical Research: Solid Earth, 123(10), 9202-9222.

LiCSBAS

LiCSBAS is an open-source package in Python and bash to carry out InSAR time series analysis using LiCSAR products (i.e., unwrapped interferograms and coherence) which are freely available on the COMET-LiCS web portal.

Users can easily derive the time series and velocity of the displacement if sufficient LiCSAR products are available in the area of interest. LiCSBAS also contains visualization tools to interactively display the time series of displacement to help investigation and interpretation of the results.

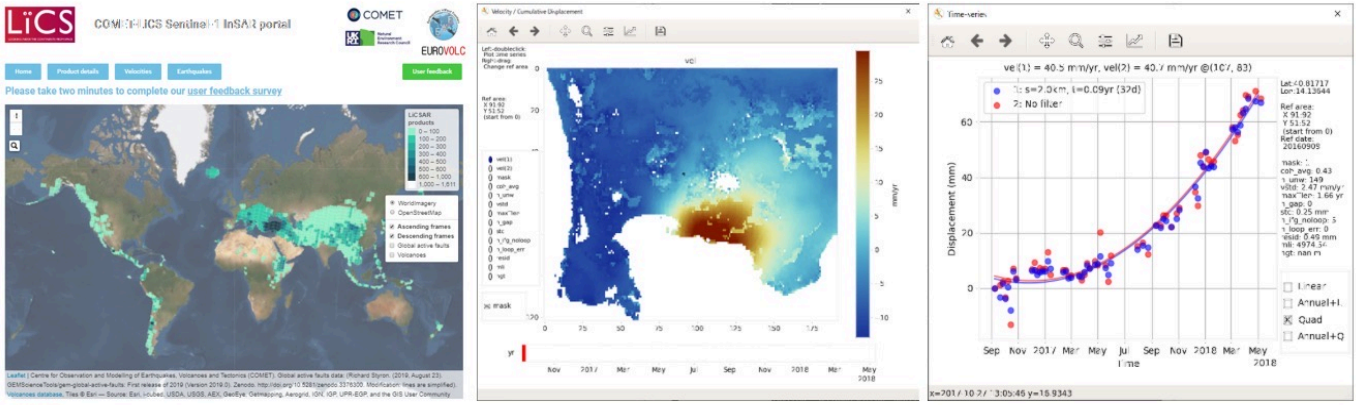

https://github.com/comet-licsar/LiCSBAS

Morishita et al., (2020). LiCSBAS: An Open-Source InSAR Time Series Analysis Package Integrated with the LiCSAR Automated Sentinel-1 InSAR Processor. *Remote Sensing*, *12*(3), 424.

Data and Methods

Sentinal-1 InSAR:

- 7 Ascending track
- 6 Descending track
- Each track includes 1 or 2 LiCSAR frames;
- Each frame uses nearly 180 epochs between October 2014 - July 2022;

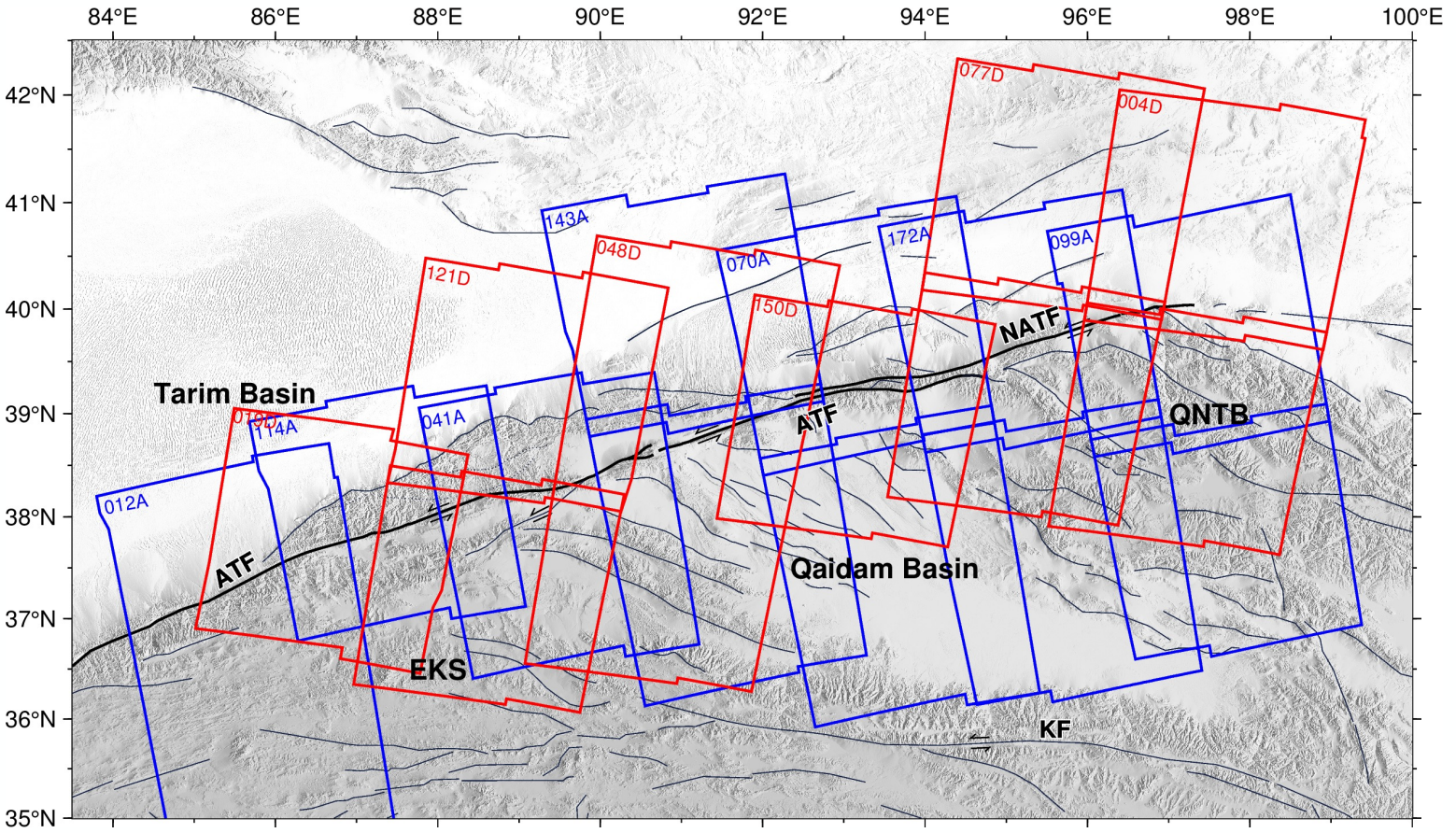

Data and Methods

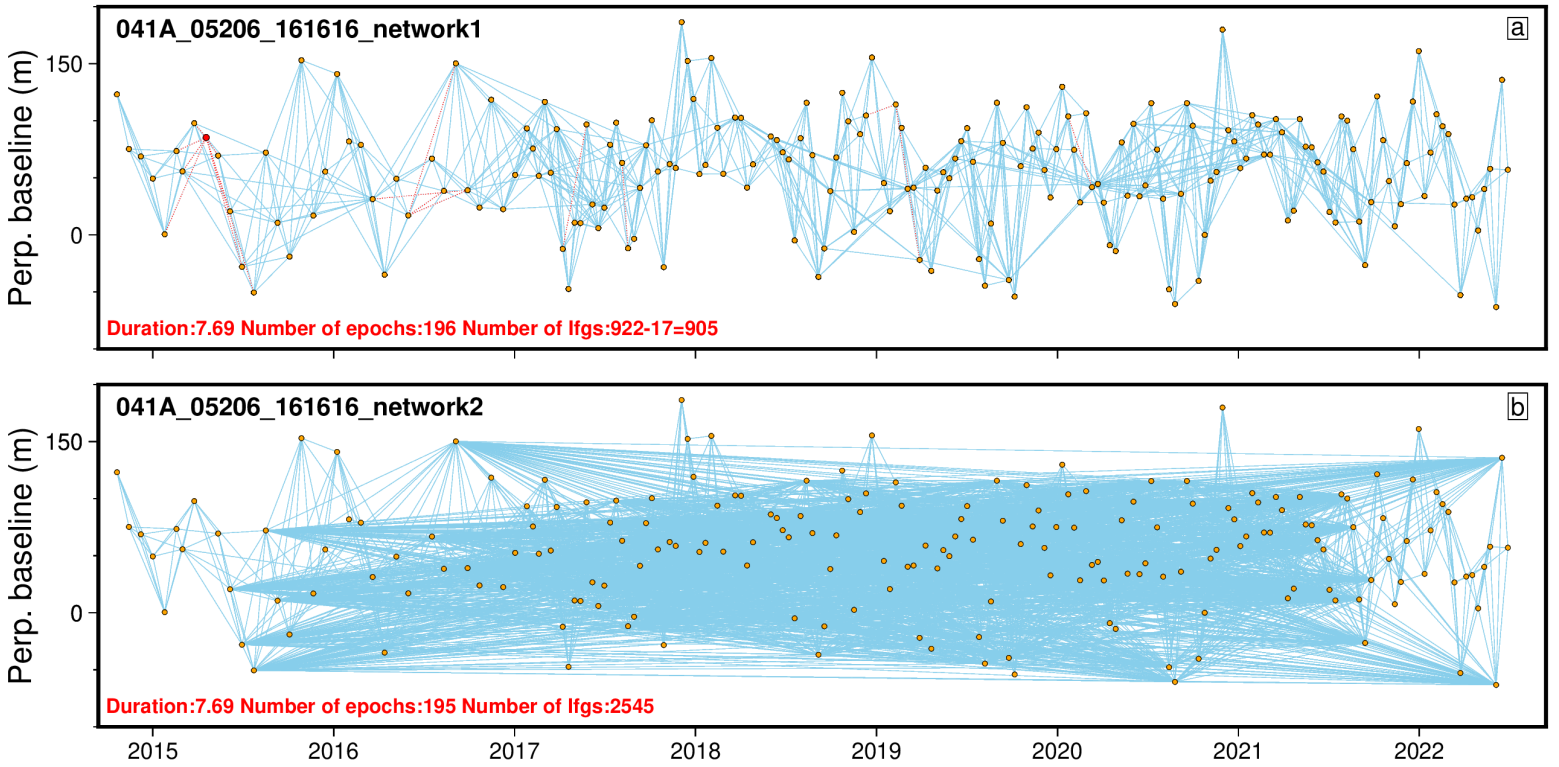

A densified network combining normal LiCS network with 1-year to 7-year long temporal summer-to-summer baselines

Benefits:

1. Reduce potential phase biases related to relatively short temporal baselines;
2. Reduce the impact of snow cover in winter;
3. Compatible with our aggressive nullifying strategy.

Data and Methods

Frame	Time Span	No. of Images	No. of Ifgs
012A_05350_242424	20141018~20220626	189	2325
114A_05193_131313	20141106~20220621	184	2293
041A_05206_161616	20141020~20220628	195	2545
143A_04999_131313	20141015~20220611	190	2466
143A_05225_171616	20150612~20220611	185	2486
070A_05026_131313	20141022~20220630	182	2167
070A_05251_161617	20141022~20211009	152	1575
172A_05014_131313	20141017~20220613	172	1863
172A_05237_161616	20141017~20220613	172	1926
099A_05018_131313	20141012~20220503	180	1868
099A_05217_131313	20150703~20220503	171	1834

Data and Methods

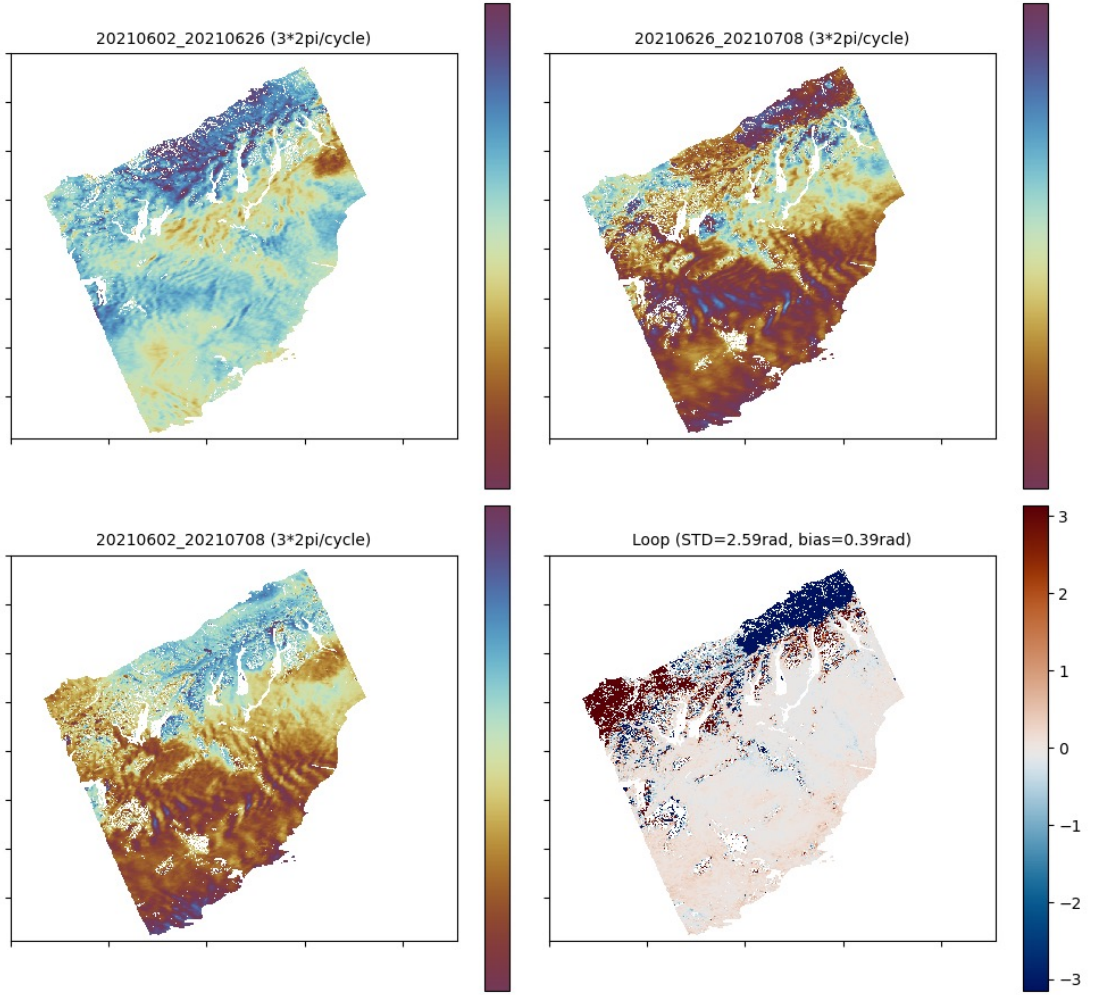

The loop closure phase of three images is calculated using the following equation:

$$\boldsymbol{\Phi_{123} = \phi_{12} + \phi_{23} - \phi_{13}}$$

where ϕ_{12}, ϕ_{23}, ϕ_{13} are the phase difference for a pixel in the interferogram between epochs ϕ_1, ϕ_2, ϕ_3.

Data and Methods

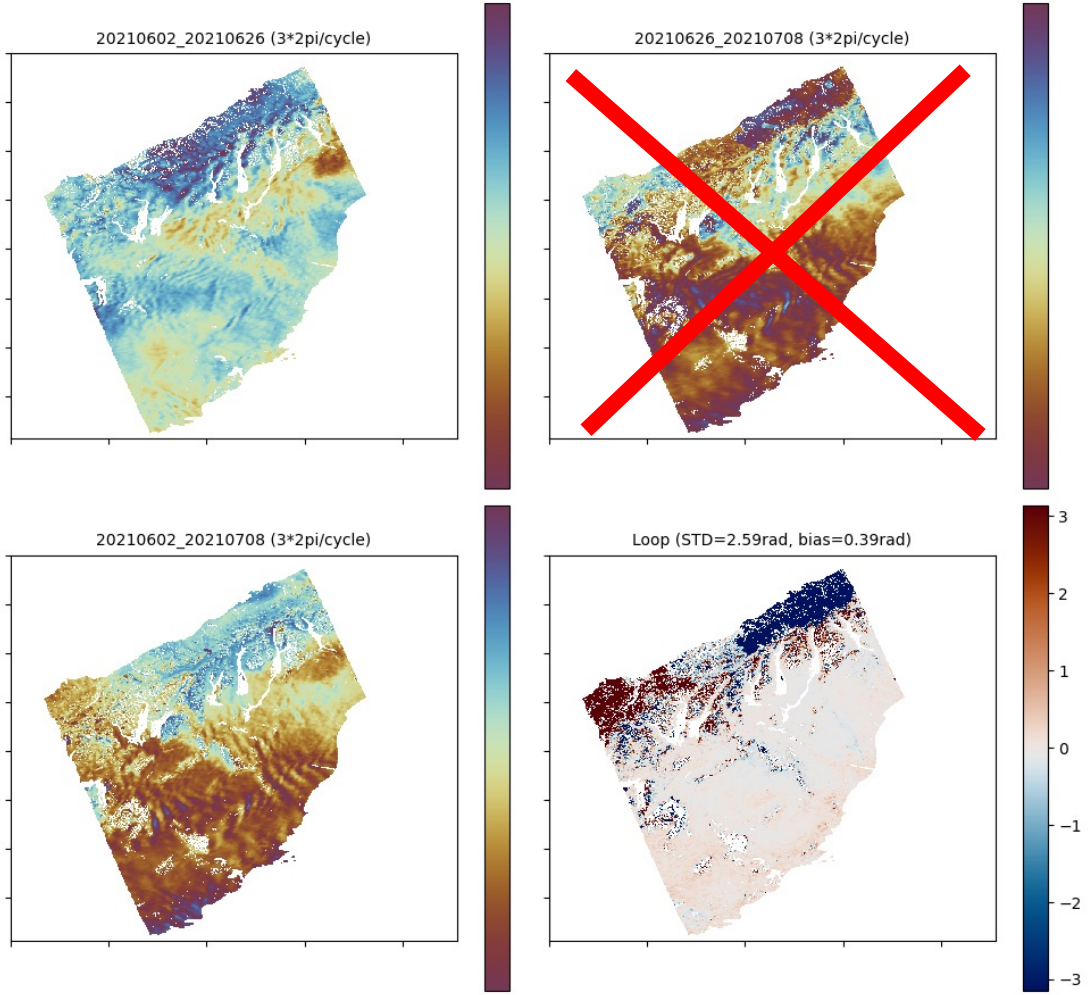

Abandon the whole interferogram based on the root mean square (RMS) of the loop phase images

(**Normally used in LiCSBAS**)

Data and Methods

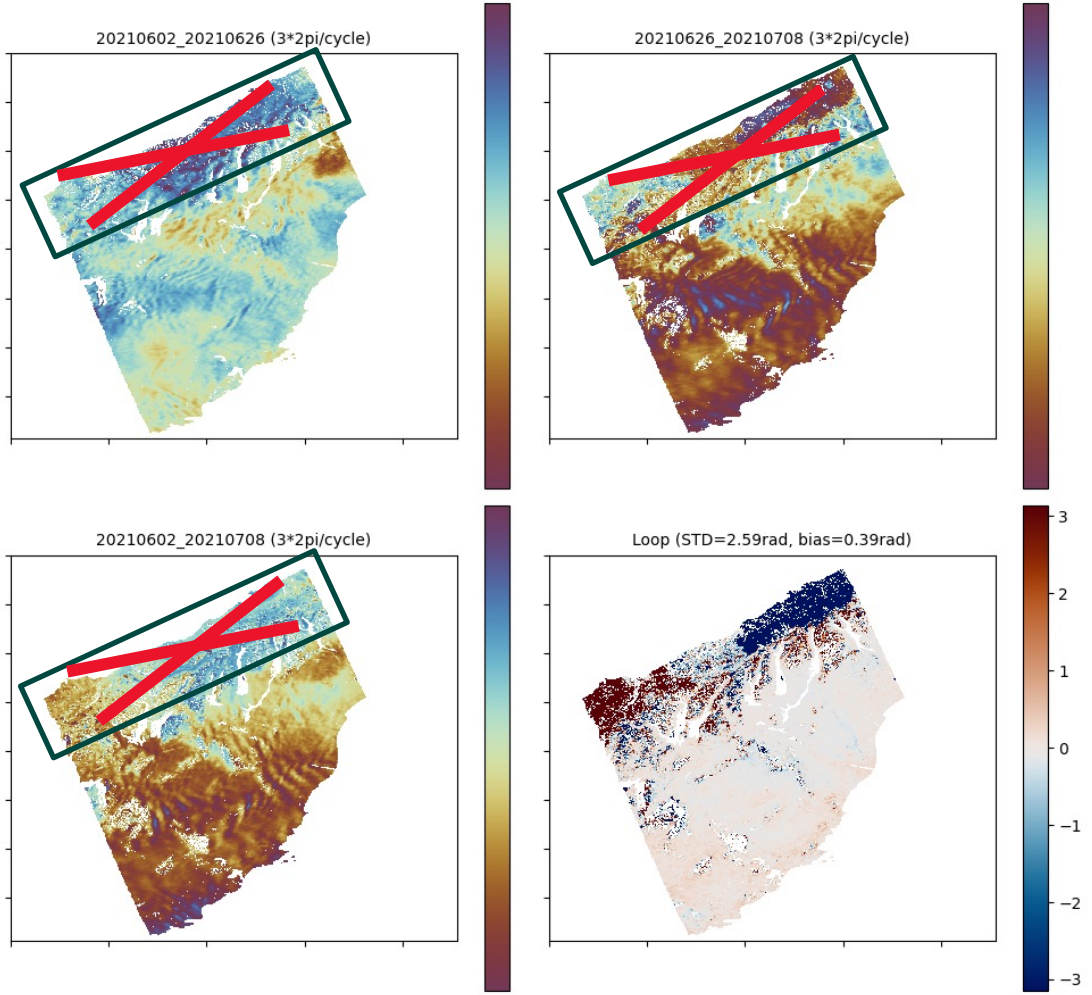

Abandon all the pixels in the interferograms

that related to unclosed loops

(**used in this research**)

Data and Methods

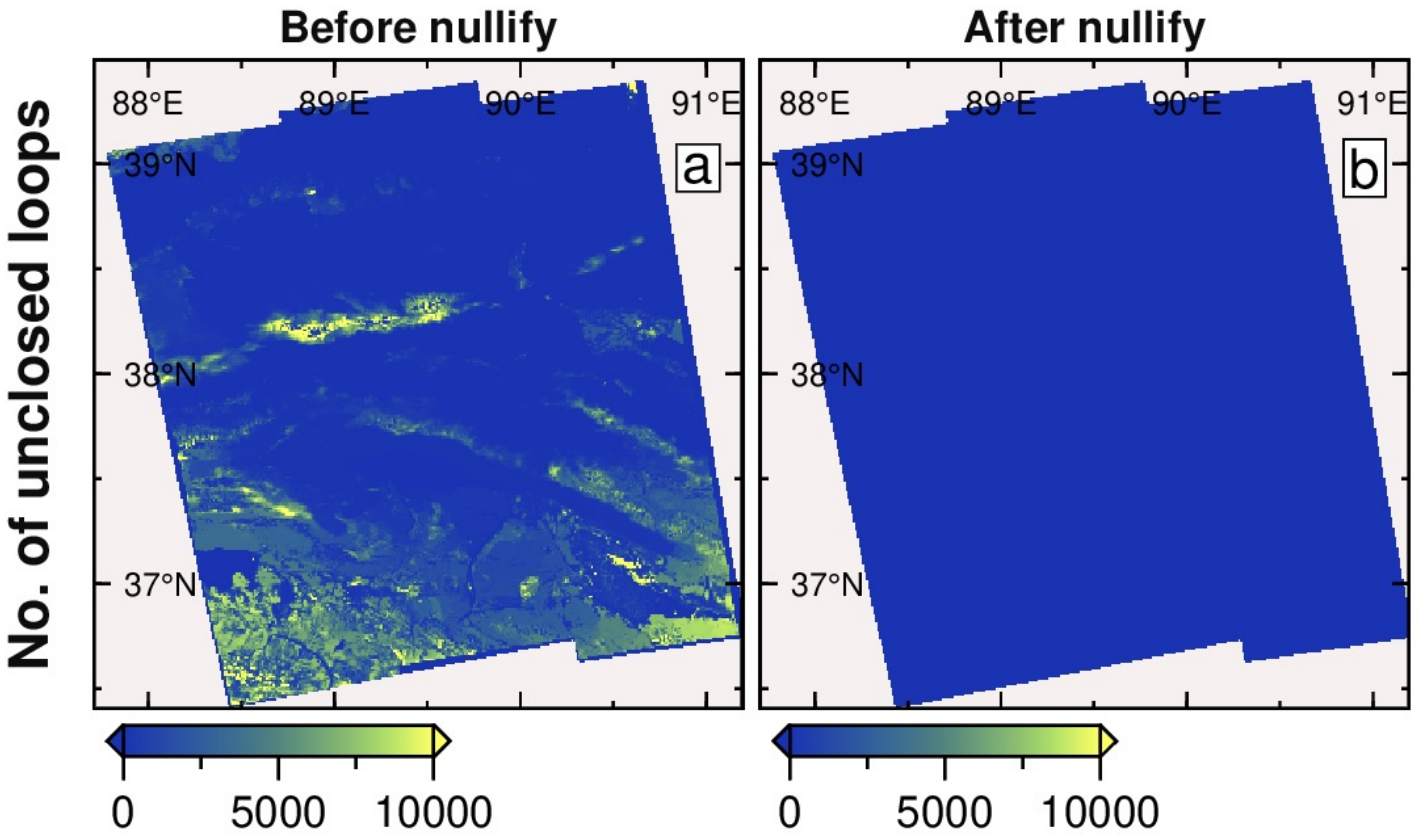

Benefits:

1. Escape nearly all the unwrapping errors;
2. Keep more interferograms;
3. Better coverage;
4. Low uncertainty in final velocities;

Data and Methods

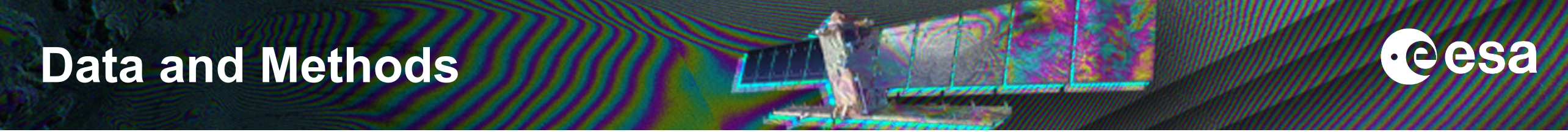

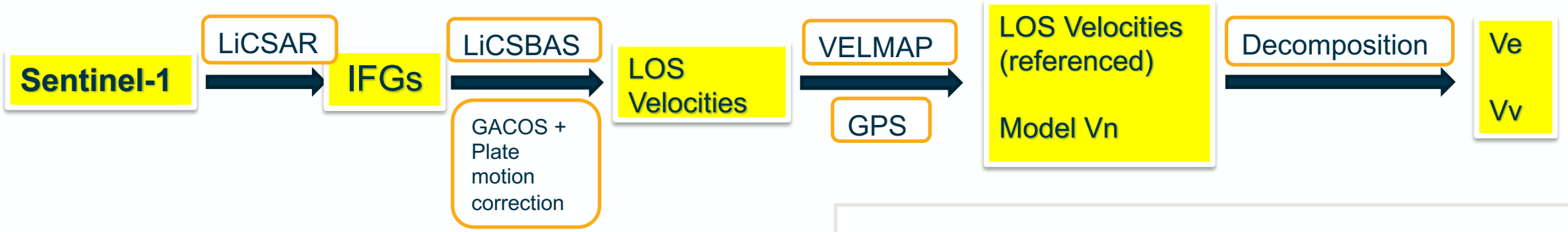

VELMAP inversion equation (Wang & Wright, 2012):

$$\begin{bmatrix} G_{sar} & G_{orb} & G_{atm} \\ G_{gps} & 0 & 0 \\ \kappa^2\nabla^2 & 0 & 0 \end{bmatrix} \begin{bmatrix} m_{vel} \\ m_{ram} \\ m_{atm} \end{bmatrix} = \begin{bmatrix} d_{sar} \\ d_{gps} \\ 0 \end{bmatrix}$$

d is the given velocities, G is the design matrix, m is the model solution, ∇^2 is the Laplacian smoothing operator approximated by a scale- dependent umbrella operator (Desbrun et al., 1999) and the factor κ^2 determines the weight of smoothing.

Velocity decomposition equation (Watson et al., 2022):

$$V_{los} = [\sin(\theta)\cos(\alpha) - \sin(\theta)\sin(\alpha) - \cos(\theta)] \begin{bmatrix} V_e \\ V_n \\ V_v \end{bmatrix}$$

where θ is the radar incidence angle, measured from the vertical to the LOS, and α is the satellite bearing.

Core References:

LiCSAR-Lazecký et al. (2020)
LiCSBAS-Morishita et al. (2020)
GACOS-Yu et al. (2018)
Plate motion correction- Stephenson et al. (2022)
VELMAP-Wang & Wright (2012)

Data and Methods

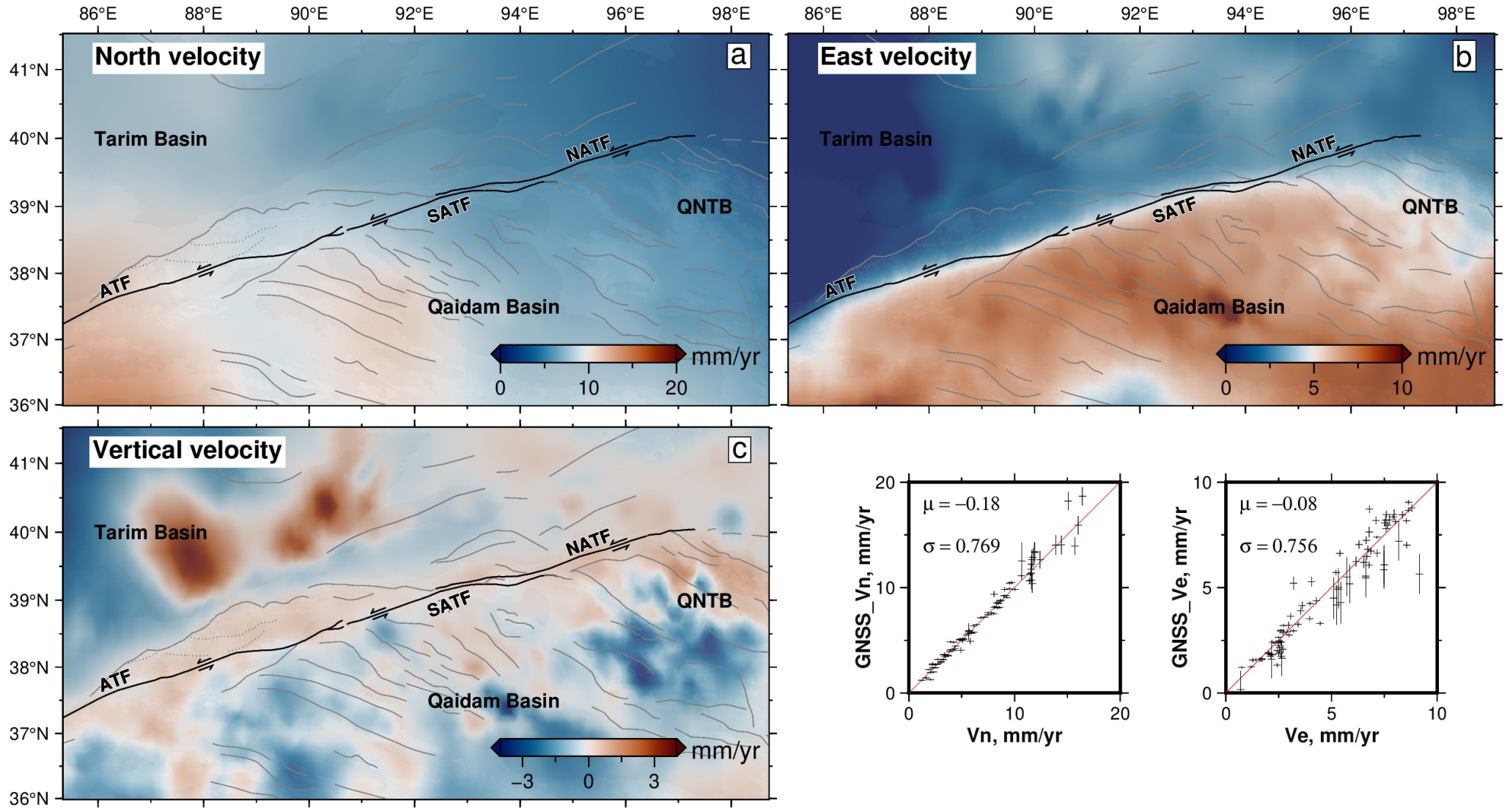

Results

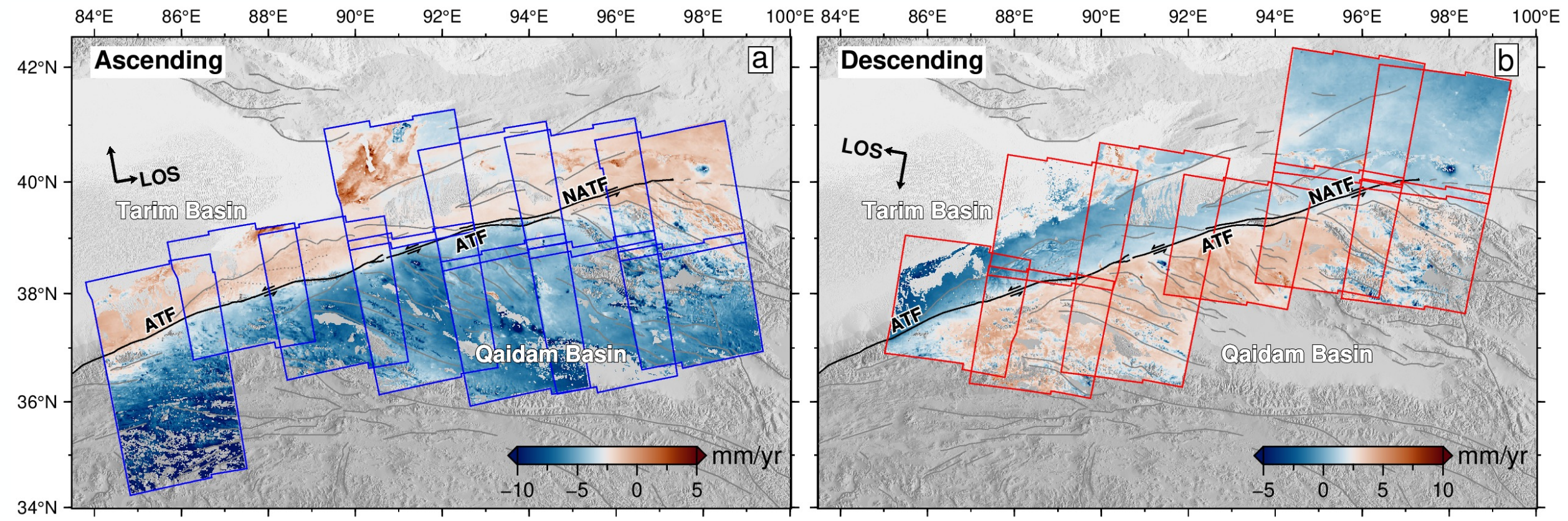
Ascending
a
LOS
Tarim Basin
NATF
ATF
ATF
Qaidam Basin
mm/yr
−10 −5 0 5
Descending
b
LOS
Tarim Basin
NATF
ATF
ATF
Qaidam Basin
mm/yr
−5 0 5 10
84°E 86°E 88°E 90°E 92°E 94°E 96°E 98°E 100°E
42°N
40°N
38°N
36°N
34°N

Results

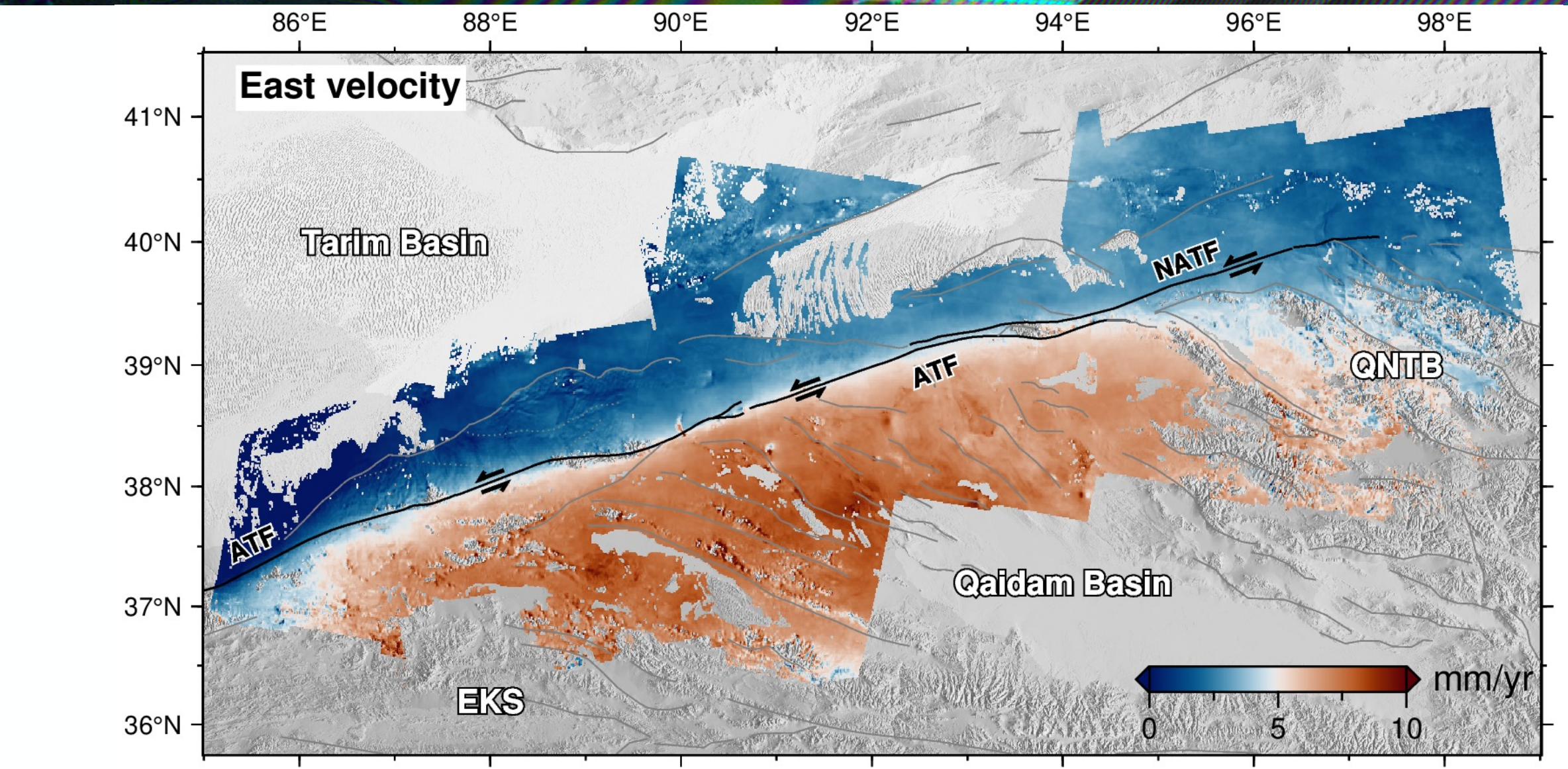
East velocity
86°E
88°E
90°E
92°E
94°E
96°E
98°E
41°N
40°N
39°N
38°N
37°N
36°N
Tarim Basin
NATF
ATF
ATF
QNTB
Qaidam Basin
EKS
mm/yr
0
5
10

Results

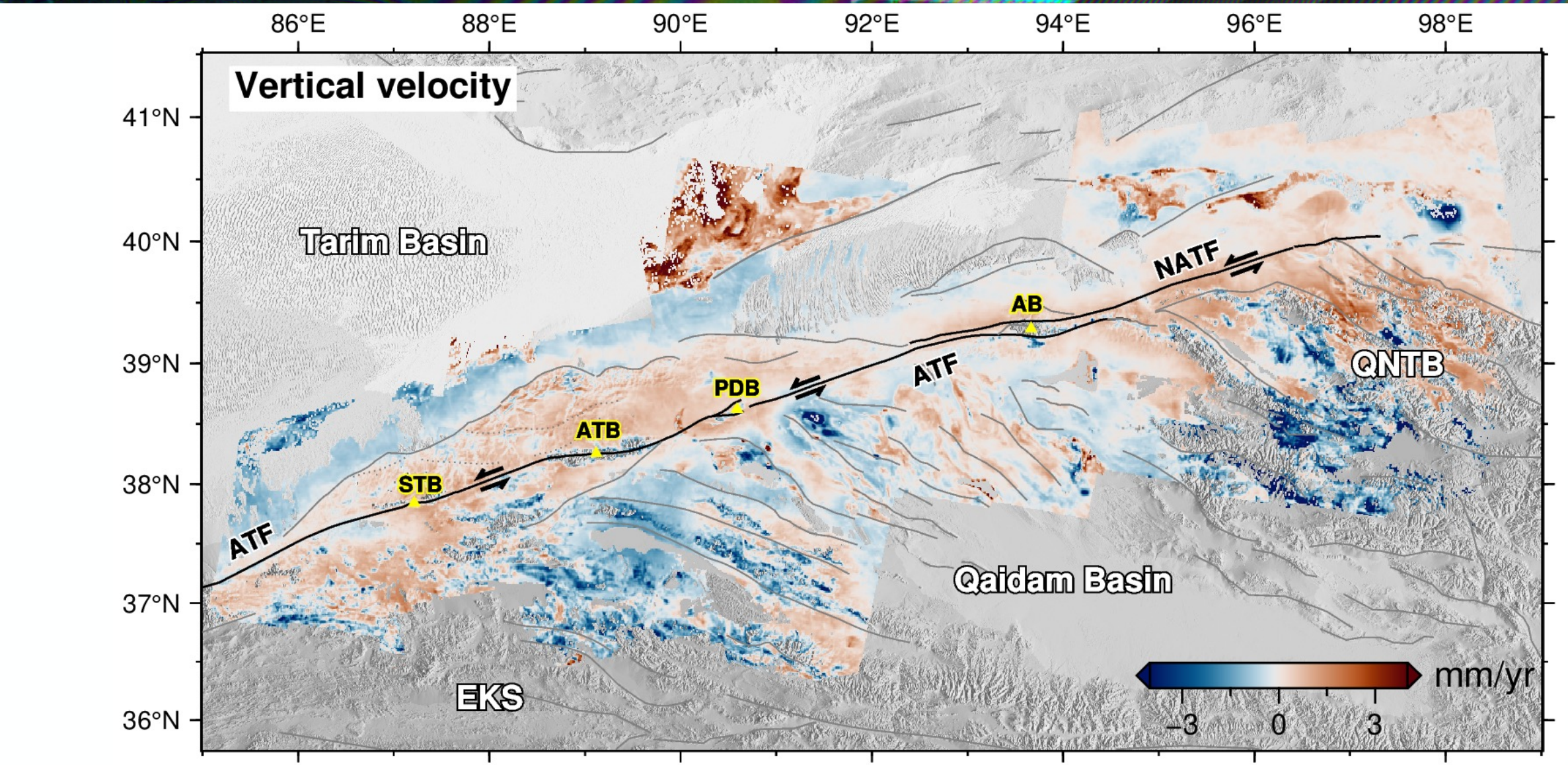
Vertical velocity
86°E
88°E
90°E
92°E
94°E
96°E
98°E
41°N
40°N
39°N
38°N
37°N
36°N
Tarim Basin
NATF
AB
ATF
PDB
ATB
STB
ATF
QNTB
Qaidam Basin
EKS
mm/yr
−3
0
3

Results

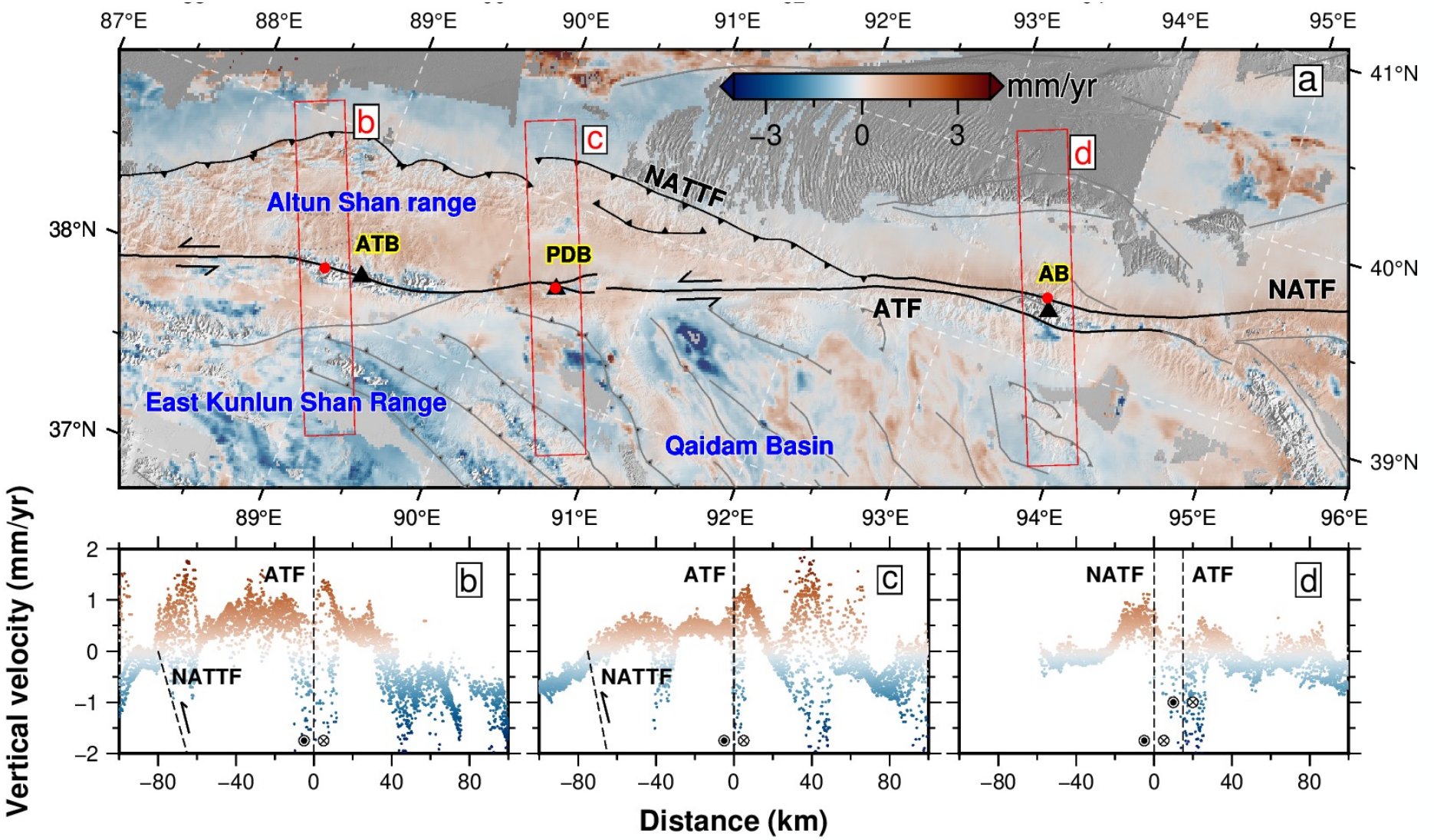
87°E
88°E
89°E
90°E
91°E
92°E
93°E
94°E
95°E
41°N
40°N
39°N
38°N
37°N
mm/yr
−3
0
3
a
b
c
d
Altun Shan range
East Kunlun Shan Range
Qaidam Basin
ATB
PDB
AB
NATTF
ATF
NATF
89°E
90°E
91°E
92°E
93°E
94°E
95°E
96°E
Vertical velocity (mm/yr)
2
1
0
−1
−2
ATF
NATTF
b
c
d
−80
−40
0
40
80
Distance (km)

Results

Finite-element modeling

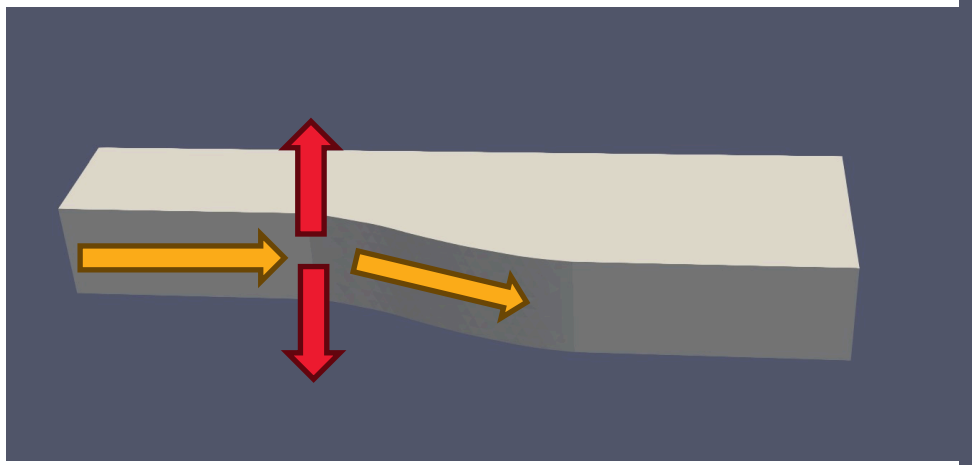

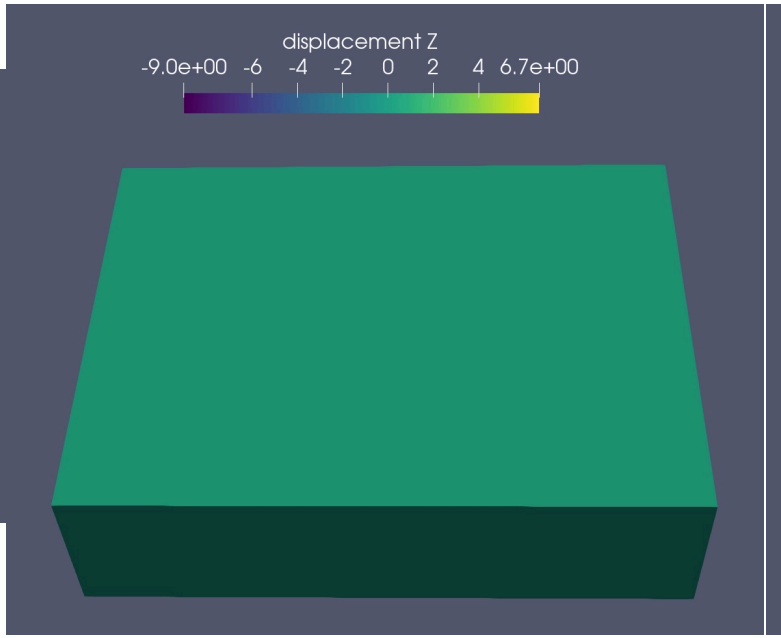

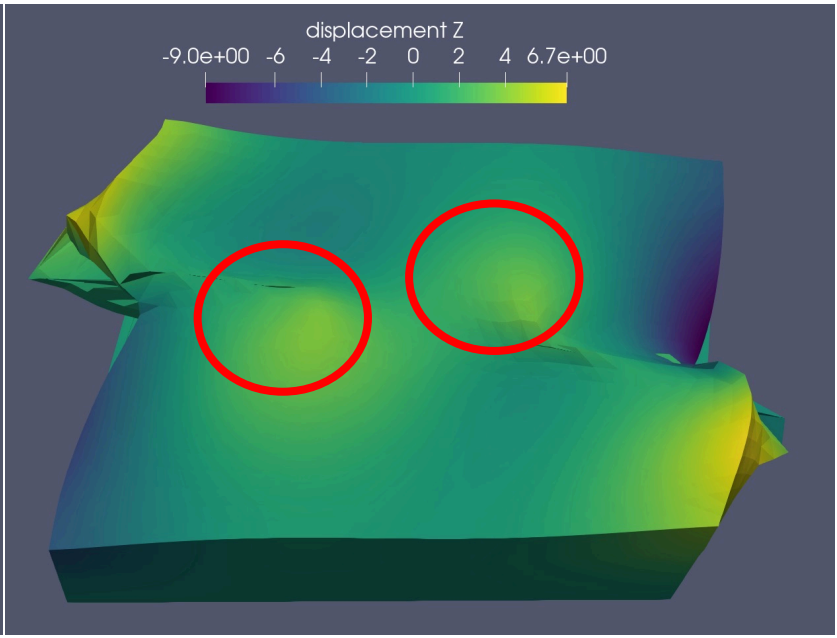

Based on Pylith
(Aagaard, B., M. Knepley, C. Williams (2022))

Results

Strain rate calculation:

$$\dot{\varepsilon}_h = \begin{bmatrix} \dot{\varepsilon}_{xx} & \dot{\varepsilon}_{xy} \\ \dot{\varepsilon}_{yx} & \dot{\varepsilon}_{yy} \end{bmatrix} = \begin{bmatrix} \dfrac{\partial V_E}{\partial x} & \dfrac{1}{2}\left(\dfrac{\partial V_E}{\partial y} + \dfrac{\partial V_N}{\partial x}\right) \\ \dfrac{1}{2}\left(\dfrac{\partial V_N}{\partial x} + \dfrac{\partial V_E}{\partial y}\right) & \dfrac{\partial V_N}{\partial y} \end{bmatrix}$$

$$\dot{\varepsilon}_{dil} = \dot{\varepsilon}_{xx} + \dot{\varepsilon}_{yy}$$

$$\dot{\varepsilon}_{shear} = \sqrt{\dot{\varepsilon}_{xy}{}^2 + \frac{\left(\dot{\varepsilon}_{xx} - \dot{\varepsilon}_{yy}\right)^2}{4}}$$

$$\dot{\varepsilon}_{II_h} = \sqrt{\dot{\varepsilon}_{xx}{}^2 + 2\dot{\varepsilon}_{xy}{}^2 + \dot{\varepsilon}_{yy}{}^2}$$

Ou et al., 2022

where $\dot{\varepsilon}_h$ is the horizontal strain-rate tensor, $\dot{\varepsilon}_{dil}$ is the horizontal dilatation rate, $\dot{\varepsilon}_{shear}$ is the maximum shear rate, $\dot{\varepsilon}_{II_h}$ is the second invariant of the horizontal strain-rate tensor, $\dot{\varepsilon}_{xx}$ represents strain in xx direction and $\frac{\partial V_E}{\partial x}$ represents velocity gradients.

Results

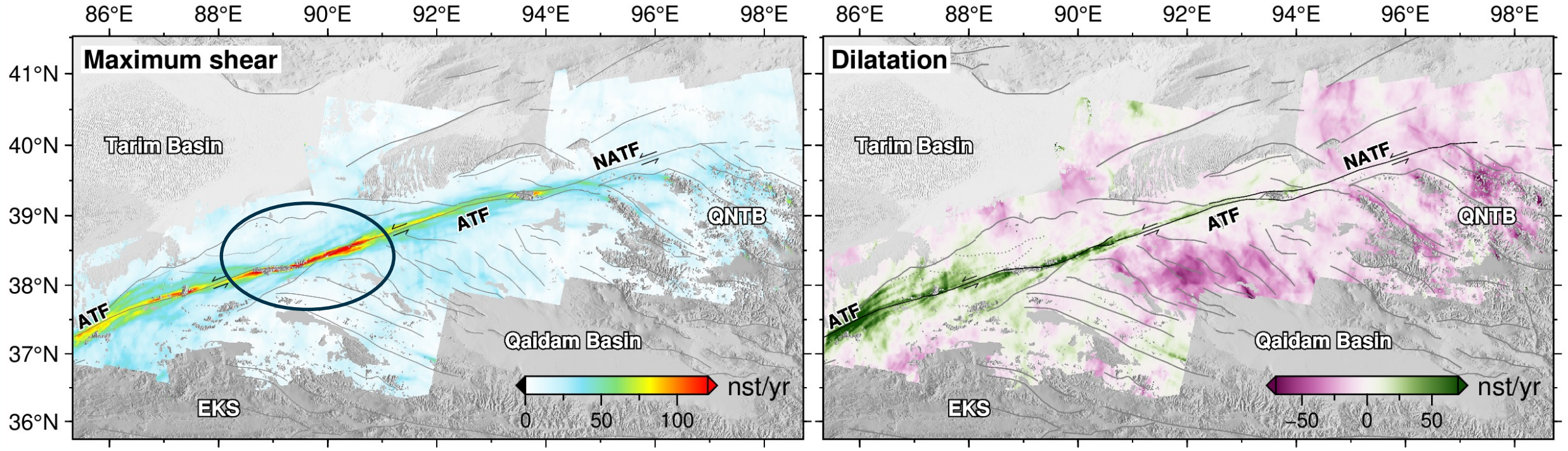
Maximum shear
Dilatation
Tarim Basin
Qaidam Basin
EKS
ATF
NATF
QNTB
nst/yr
0
50
100
−50
0
50
86°E
88°E
90°E
92°E
94°E
96°E
98°E
41°N
40°N
39°N
38°N
37°N
36°N

Results

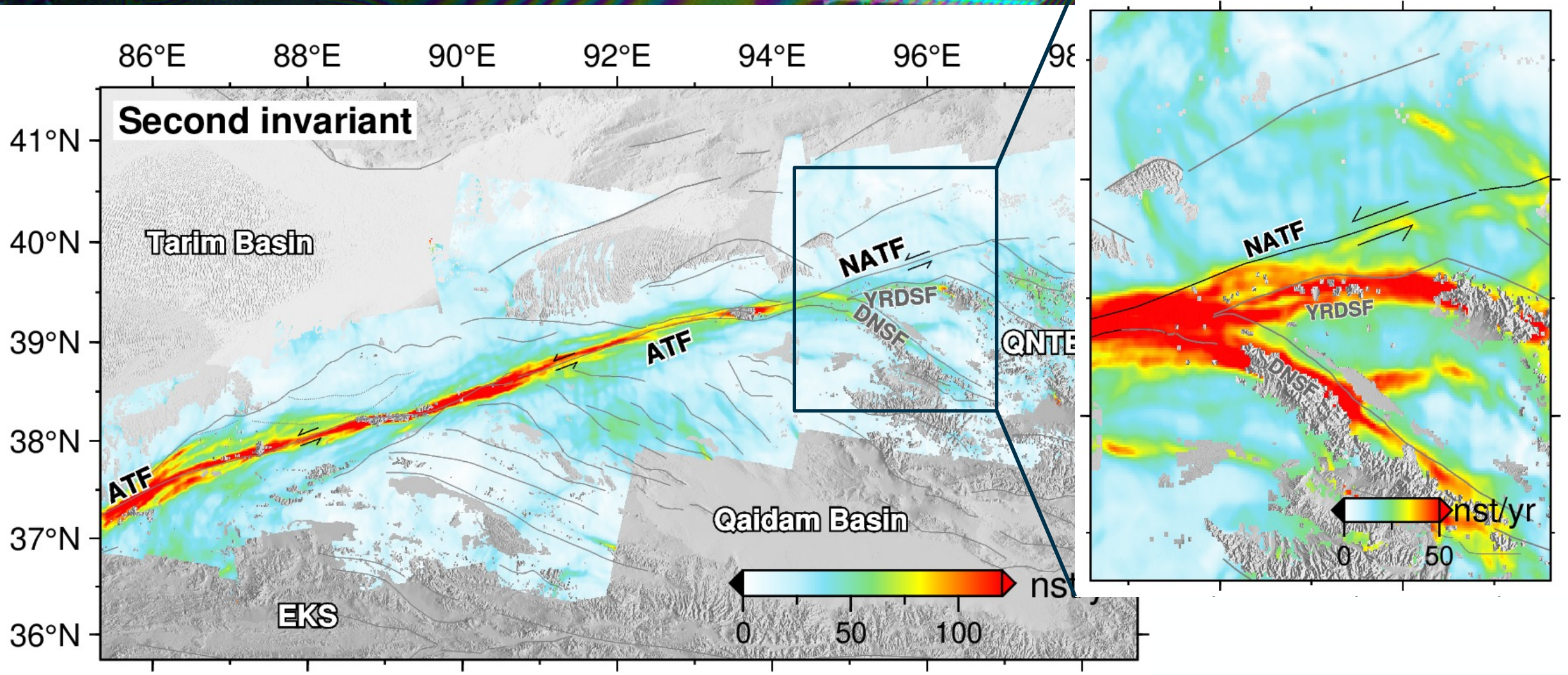
86°E
88°E
90°E
92°E
94°E
96°E
41°N
40°N
39°N
38°N
37°N
36°N
Second invariant
Tarim Basin
ATF
ATF
NATF
YRDSF
DNSF
QNTB
Qaidam Basin
EKS
0
50
100
nst/yr
NATF
YRDSF
DNSF
nst/yr
0
50

Results

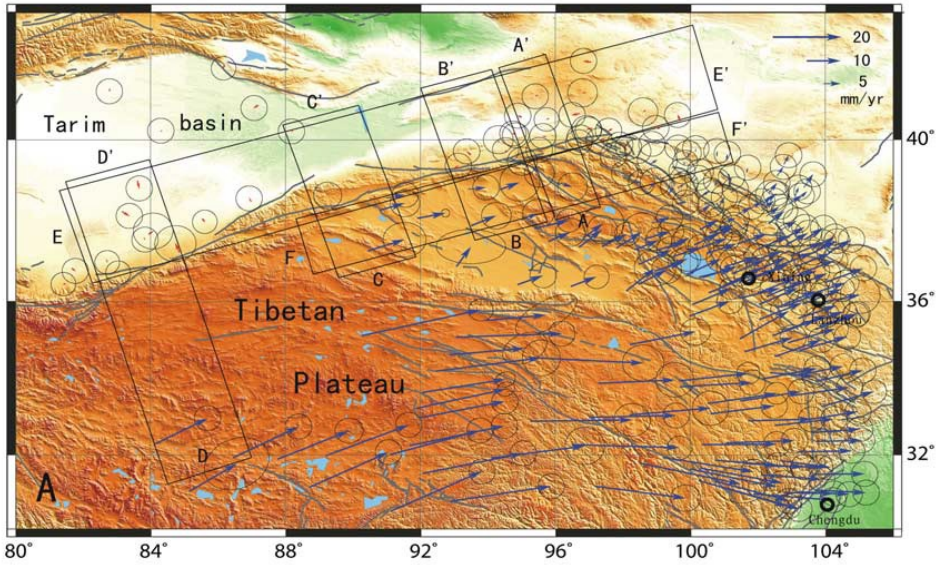

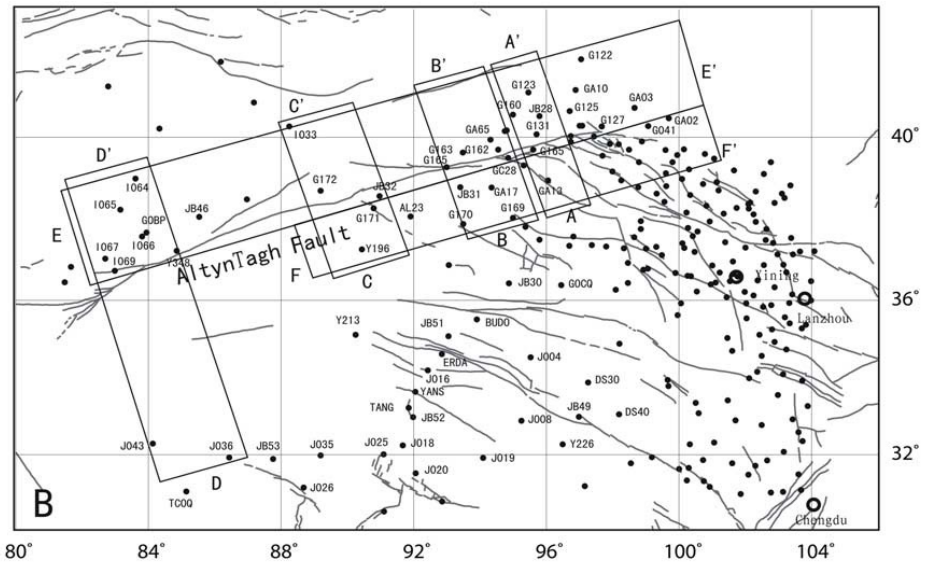

Zhang et al., 2007

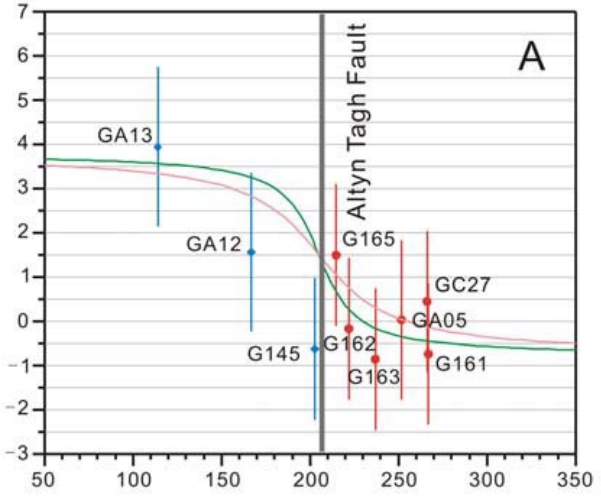

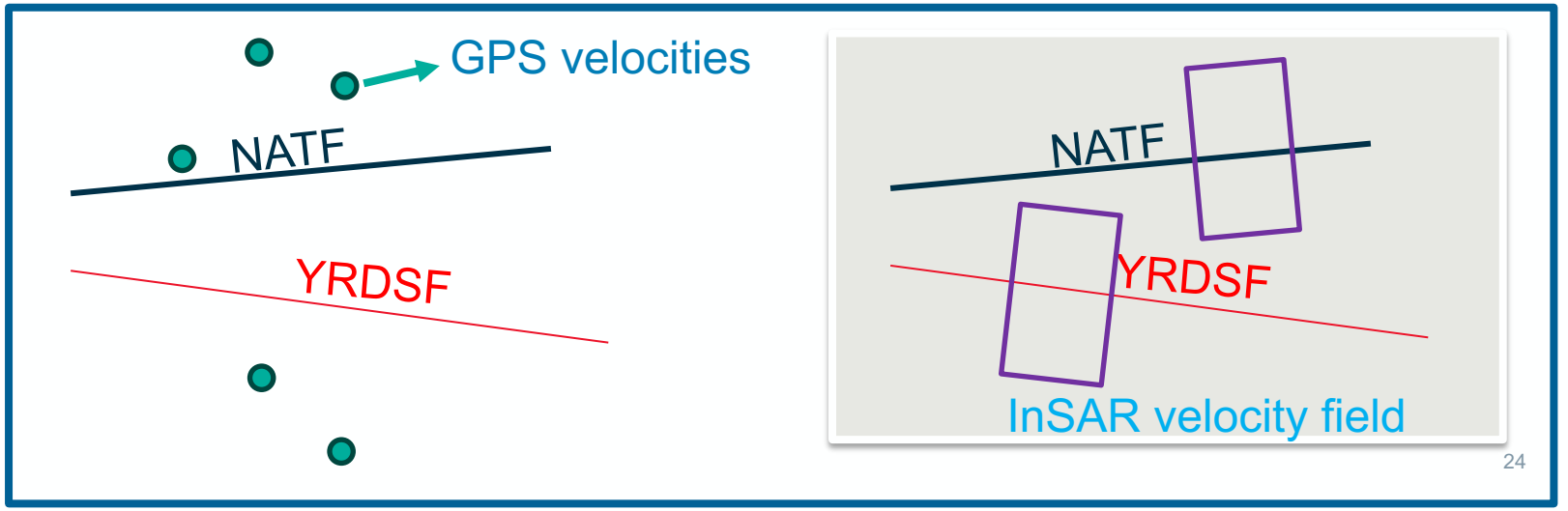

Results

$$v_{fault\_para} = \left(\frac{S}{\pi}\right)\arctan\left(\frac{x-L}{D}\right) + c$$

Savage et al, 1973

Best-fitted solution:
S=0.9±1.1; D=7.0±12.2; L=5.6±10.7 (NATF)
S=2.4±1.3; D=13.3±11.7; L=4.5±9.3 (YRDSF)

NATF

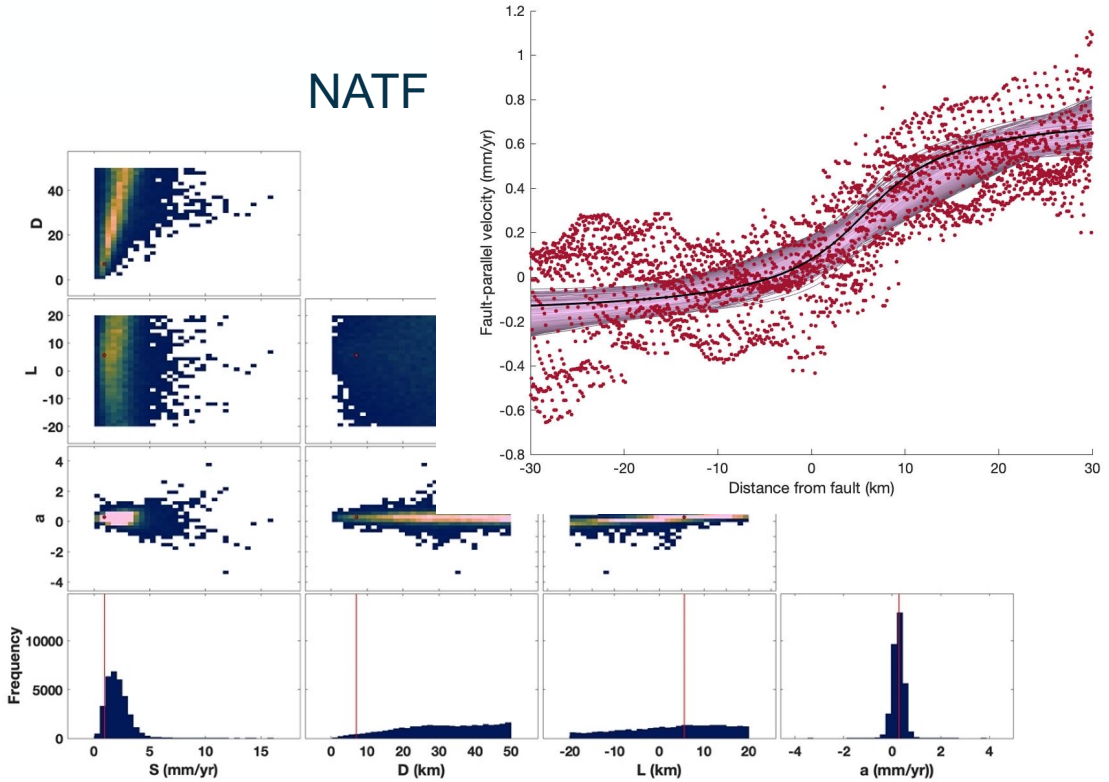

YRDSF

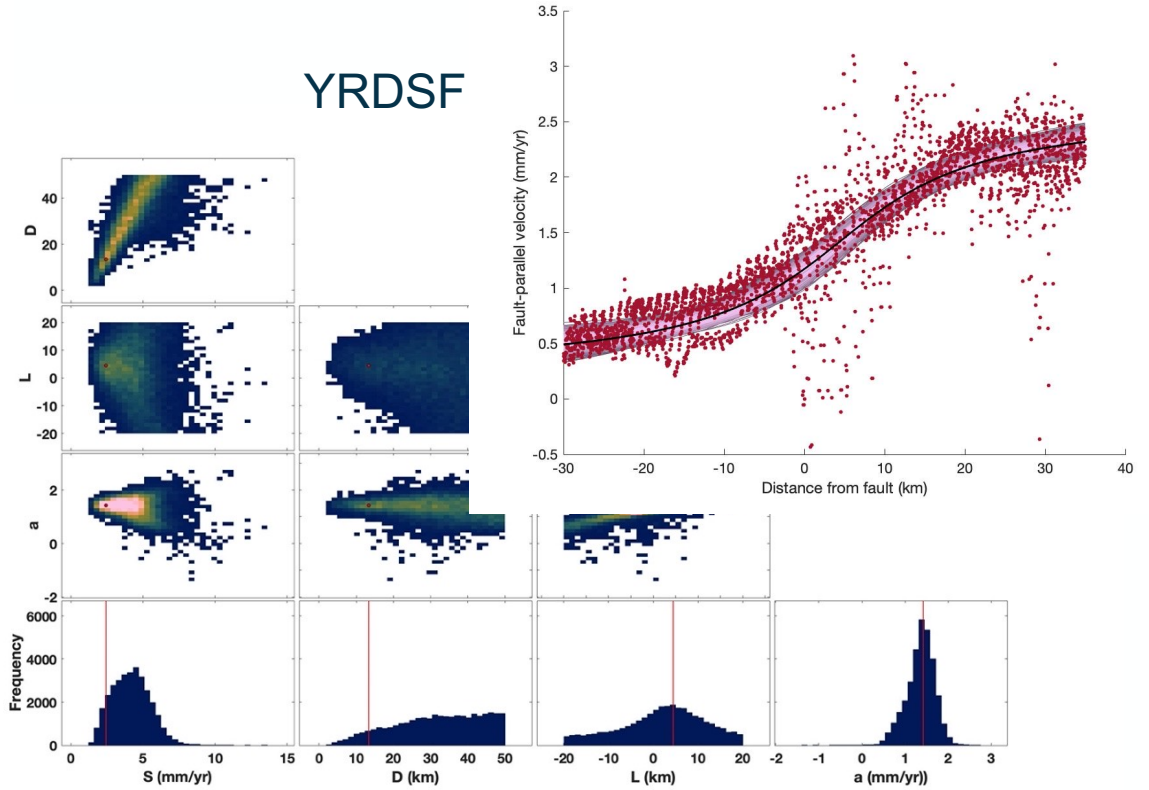

Results

Slip Rate of Yema River–Daxue Mountain Fault since the Late Pleistocene and Its Implications on the Deformation of the Northeastern Margin of the Tibetan Plateau

LUO Hao[1, 2], HE Wengui[2, 3, *], YUAN Daoyang[2, 3] and SHAO Yanxiu[2, 3]

1 *Key Laboratory of Active Tectonics and Volcano, Institute of Geology, China Earthquake Administration, Beijing 100029, China*
2 *Lanzhou Institute of Seismology, China Earthquake Administration, Lanzhou 730000, China*
3 *Lanzhou National Geophysical Observatory, Lanzhou 730000, China*

Abstract: The slip rate of Yema River–Daxue Mountain fault in the western segment of Qilian Mountains was determined by the dated offset of river risers or gullies. Results indicate that the left-lateral fault slip rate is 2.82 ± 0.20 mm/a at Dazangdele site, 2.00 ± 0.24 mm/a at Shibandun site, and 0.50 ± 0.36 and 2.80 ± 0.33 mm/a at two sites in Zhazihu. The ideal average slip rate of the whole fault is 2.81 ± 0.32 mm/a. The lower slip rate confirms part of the displacement of Altyn Tagh fault was transformed into an uplifting of the strap mountains in the western segment of Qilian Mountains, whereas another part transformed into sinistral displacement of Haiyuan fault. This study illustrates that the slip of large strike-slip faults in the northeastern margin of the plateau transforms into crust thickening at the tip of the fault without large-scale propagation to the outer parts of the plateau.

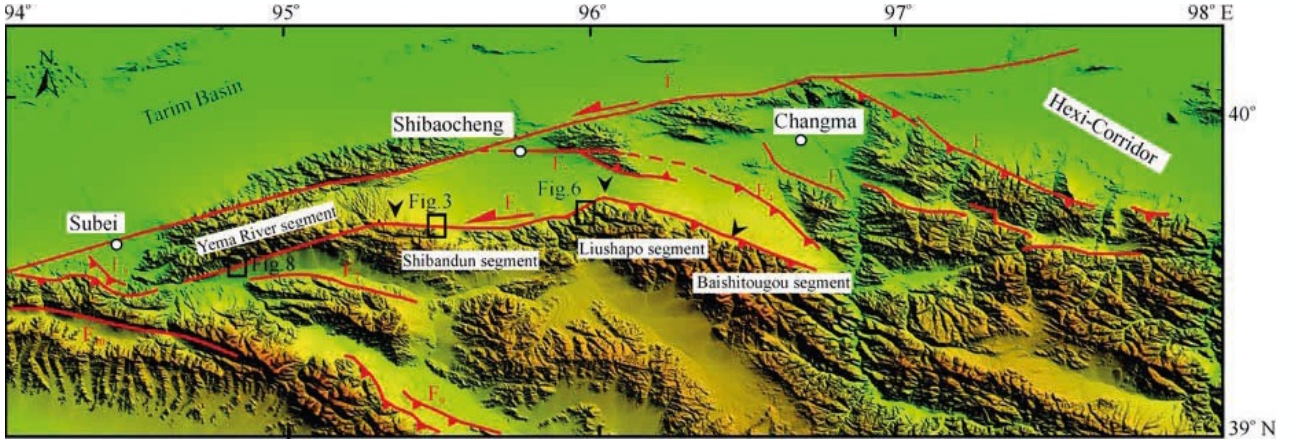

Luo, H., He, W., Yuan, D., Shao, Y., 2015. Slip Rate of Yema River-Daxue Mountain Fault since the Late Pleistocene and Its Implications on the Deformation of the Northeastern Margin of the Tibetan Plateau. *Acta Geologica Sinica*. 89(2), 561–574. https://doi.org/10.1111/1755-6724.12447.

Results

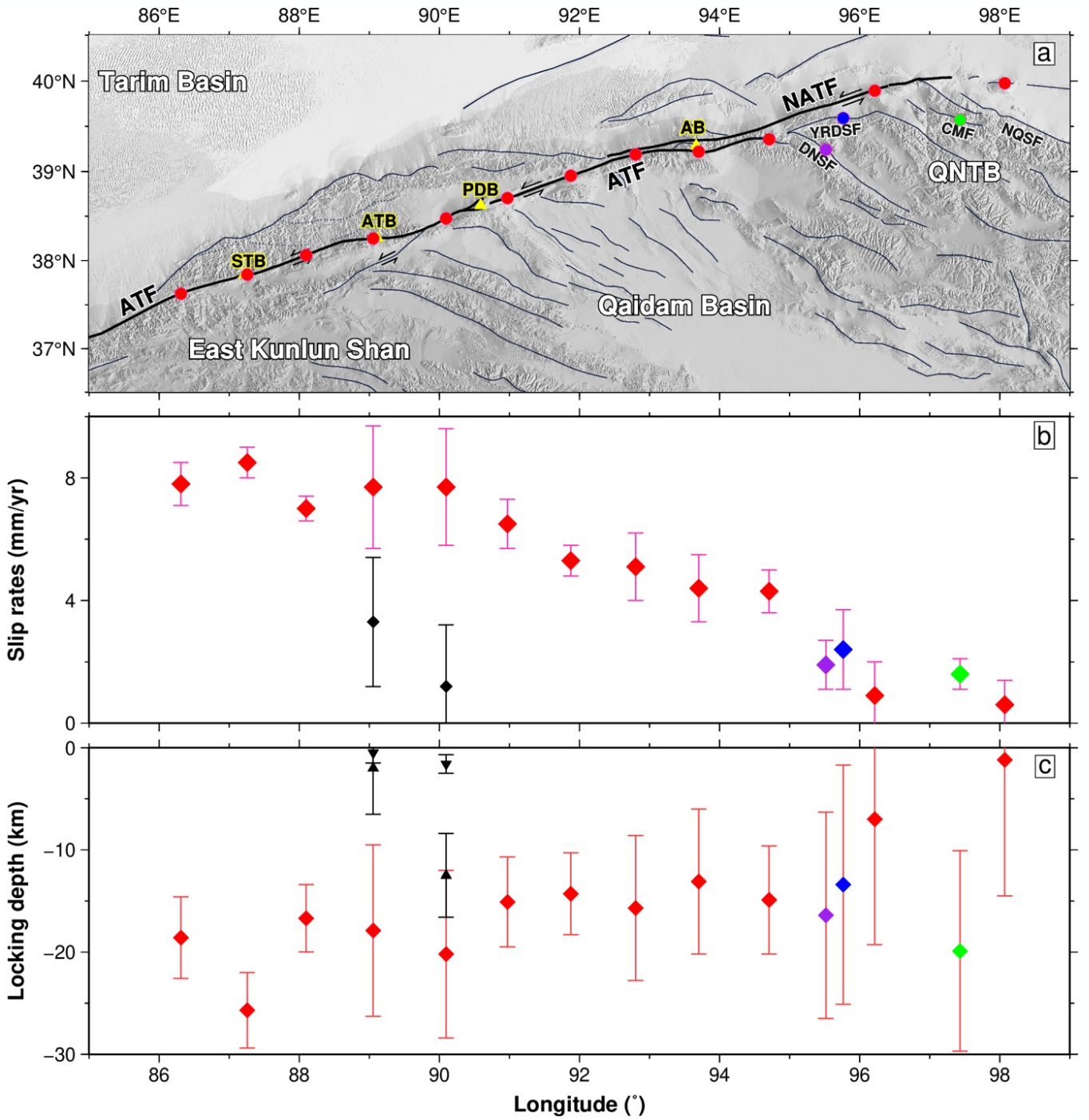
a
Tarim Basin
East Kunlun Shan
Qaidam Basin
QNTB
ATF
NATF
AB
PDB
ATB
STB
YRDSF
DNSF
CMF
NQSF
86°E
88°E
90°E
92°E
94°E
96°E
98°E
40°N
39°N
38°N
37°N
b
Slip rates (mm/yr)
c
Locking depth (km)
Longitude (°)

Conclusions

- A pixel-based aggressive nullifying method can be used to escape the unwrapping errors during the time series analysis.

- A 3D velocity map has been obtained in our study, and this can be used to reveal the spatial variation of strain accumulation and mountain growth along the central-eastern ATF.

- Important strain partitioning along the central-eastern ATF can be revealed through strain rate maps, which should be considered carefully in future interpretation.

Thanks

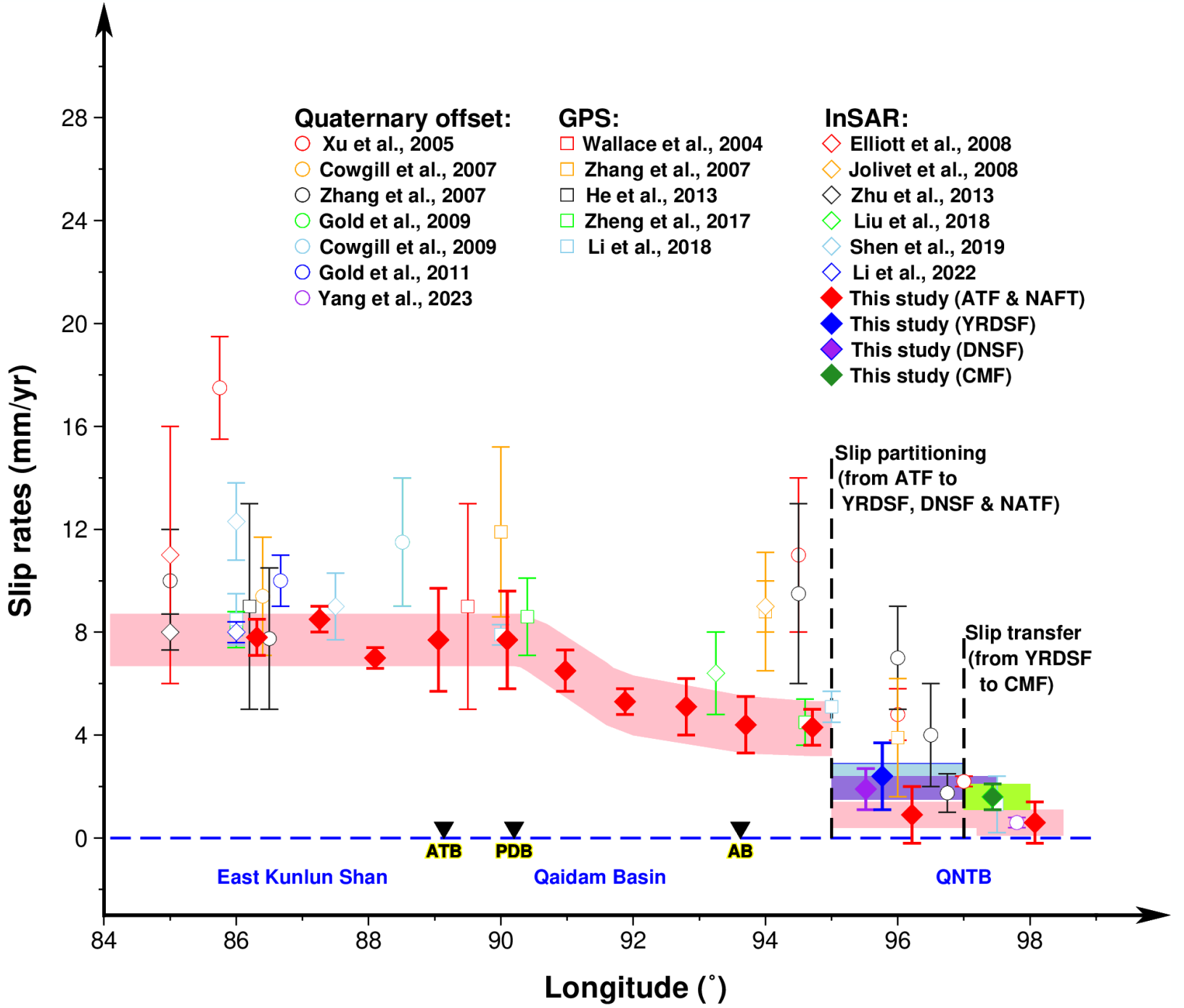
Quaternary offset:
Xu et al., 2005
Cowgill et al., 2007
Zhang et al., 2007
Gold et al., 2009
Cowgill et al., 2009
Gold et al., 2011
Yang et al., 2023
GPS:
Wallace et al., 2004
Zhang et al., 2007
He et al., 2013
Zheng et al., 2017
Li et al., 2018
InSAR:
Elliott et al., 2008
Jolivet et al., 2008
Zhu et al., 2013
Liu et al., 2018
Shen et al., 2019
Li et al., 2022
This study (ATF & NAFT)
This study (YRDSF)
This study (DNSF)
This study (CMF)
Slip partitioning
(from ATF to
YRDSF, DNSF & NATF)
Slip transfer
(from YRDSF
to CMF)
ATB
PDB
AB
East Kunlun Shan
Qaidam Basin
QNTB
Slip rates (mm/yr)
Longitude (˚)
0
4
8
12
16
20
24
28
84
86
88
90
92
94
96
98